



INELASTIC DEFORMATION OF POLYCRYSTALLINE FACE CENTERED CUBIC MATERIALS BY SLIP AND TWINNING

A. STAROSELSKY and L. ANAND*

Department of Mechanical Engineering, Massachusetts Institute of Technology, Cambridge,
MA 02139, U.S.A.

(Received 11 February 1997; in revised form 10 September 1997)

ABSTRACT

There have been considerable recent advances in the understanding of anisotropy due to crystallographic texturing, and a reasonably successful elasto-viscoplasticity theory for the deformation of face-centered-cubic (f.c.c.) single crystals and polycrystals with high stacking fault energies is now at hand. The high stacking fault energy f.c.c. materials (e.g. Cu, Al) deform predominantly by crystallographic slip. In contrast, for materials with low stacking energies, e.g. α -brass, in addition to crystallographic slip, deformation twinning plays an important role in maintaining generalized plastic flow. A direct manifestation of twinning is the different crystallographic texture that is observed in 70–30 brass as compared to pure copper.

In this paper we formulate a rate-independent constitutive model which accounts for both slip and twinning. We have also developed a new scheme to determine the active systems and the shear increments on the active slip and twin systems. We have implemented our constitutive equations and computational procedures in the finite-element program ABAQUS/Explicit (1995).

By using comparisons between model predictions and macroscopically-measured stress–strain curves and texture evolution we have deduced information about the values of the single-crystal parameters associated with slip and twin system deformation resistances and hardening due to slip and twinning. We show that our model is able to reproduce both the experimentally measured pole figures and the stress–strain curves in plane strain compression for α -brass. With the model so calibrated, we show that the predictions for the texture and stress–strain curves from the model are also in reasonably good agreement with experiments in simple compression.

We have also evaluated the applicability of a Taylor-type model for combined slip and twinning. Our calculations show that for the high-symmetry f.c.c. brass, a Taylor-type model for crystals deforming by combined slip and twinning is able to reasonably well predict the macroscopic stress–strain curves and crystallographic texture evolution.

Our calculations show that in plane strain as well as simple compression, the crystallographic texture that develops is a result of lattice rotation due to both slip and twinning, and that as suggested by Wassermann (1963), in contrast to copper which does not twin under normal circumstances, it is twinning which is responsible for the brass-type texture that is observed in f.c.c. metals with low stacking fault energies. © 1998 Elsevier Science Ltd. All rights reserved.

Keywords: A. twinning, B. constitutive behavior, B. crystal plasticity, C. finite elements, C. mechanical testing.

1. INTRODUCTION

In polycrystalline metals the major cause of the anisotropic plastic response is crystallographic texture resulting from the reorientation of the crystal lattices of grains

* Author to whom all correspondence should be addressed. Fax: 001 617 258 8742. E-mail: anand@mit.edu.

during deformation. There have been considerable recent advances in the understanding of anisotropy due to crystallographic texturing, and a reasonably successful, physically-based elasto-viscoplasticity theory for the deformation of f.c.c. single crystals and polycrystals with high stacking fault energies at low homologous temperatures (<0.3 of the melting temperature) and low strain rates (10^{-3} – 10^1 s $^{-1}$) is now at hand. The theory is able to predict the macroscopic anisotropic stress–strain response, shape changes and the evolution of crystallographic texture in complex deformation modes. Also, it is beginning to be applied to the analysis of deformation-processing problems under isothermal and quasi-static conditions (e.g. Mathur and Dawson, 1989, 1990; Bronkhorst *et al.*, 1992; Kalidindi *et al.*, 1992; Anand and Kalidindi, 1994; Beaudoin *et al.*, 1994; Balasubramanian and Anand, 1996).

The high stacking fault energy f.c.c. materials (e.g. Al, Cu) deform predominantly by crystallographic slip, and the recent progress in the formulation of a mathematical theory of polycrystalline plasticity has occurred primarily for materials with cubic crystals which do not twin. In contrast, for materials with low stacking energies, e.g. α -brass, in addition to crystallographic slip, deformation twinning plays an important role in maintaining generalized plastic flow.† A direct manifestation of twinning is the different crystallographic texture that is observed in 70–30 brass as compared to commercially pure copper, and this is one of the classical problems in texture research (e.g. Wasserman, 1963; Dillamore and Roberts, 1964; Smallman and Green, 1964; Goodman and Hu, 1968). Figure 1 shows a comparison of our measurements of the $\{111\}$, $\{100\}$ and $\{110\}$ pole figures in brass and copper after plane strain compression of 100%. The differences between the $\{111\}$ and $\{100\}$ pole figures of brass and copper are quite pronounced.

Another material response characteristic which is different for α -brass as compared to that for copper is the variation of the rate of strain hardening with strain. Experimentally measured stress–strain curves and the corresponding relation between the strain hardening rate $d|\sigma|/d|\epsilon|$ and true strain $|\epsilon|$ in plane-strain compression are shown in Fig. 2. For copper the rate of strain hardening decreases continuously with increasing strain (for the level of strains examined), while the rate of strain hardening for the brass exhibits a plateau at intermediate strain levels. Extensive microscopic observations by Asgari *et al.* (1997) show that the plateau in the strain hardening rate can be correlated with the onset of twinning, and it is the twin-twin and twin-slip hardening interactions which arrest the decrease in the strain hardening rate in brass at these intermediate strain levels.

The analytical modeling and computational accounting for twinning as a mechanism of inelastic deformation, texture evolution, and strain hardening is in its nascent stages. Some of the early considerations of twinning in texture development are those of Chin *et al.* (1969) and Chin and Mammel (1969). For a brief review of this early work on twinning, see Chin (1975). Twinning is a more complicated deformation mode than slip because, in addition to the twinning shear, it produces a volume fraction of the grain with a very different orientation than that of the rest of the grain;

† Venables (1964) first recognized the relationship between the susceptibility of a metal to twin and the value of its stacking fault energy. He showed that the critical resolved shear stress for twinning decreased with decreasing stacking fault energy, as occurs for example in Cu–Zn alloys with increasing amounts of zinc.

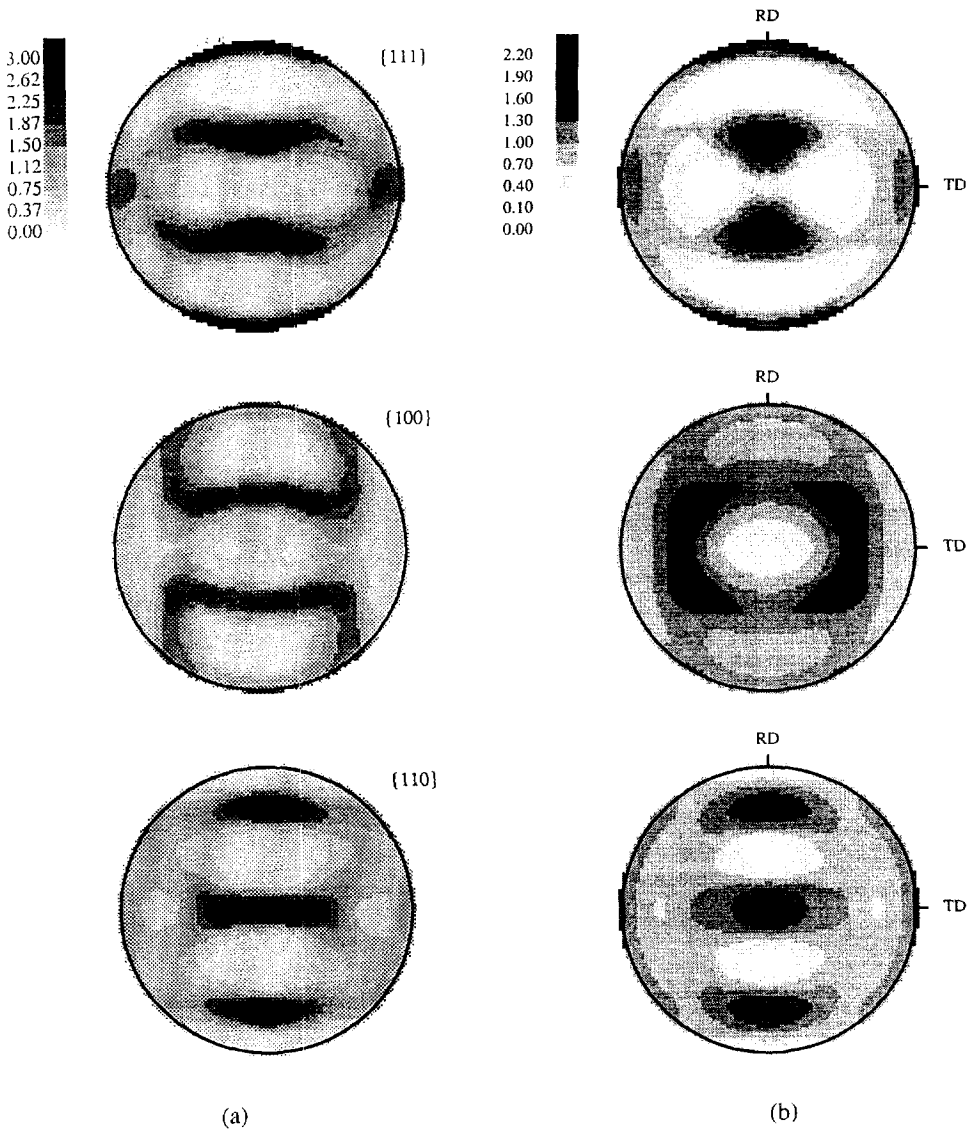


Fig. 1. Experimentally-measured crystallographic texture for (a) copper (Bronkhorst *et al.*, 1992), and (b) 70-30 brass after plane strain compression of 100%.

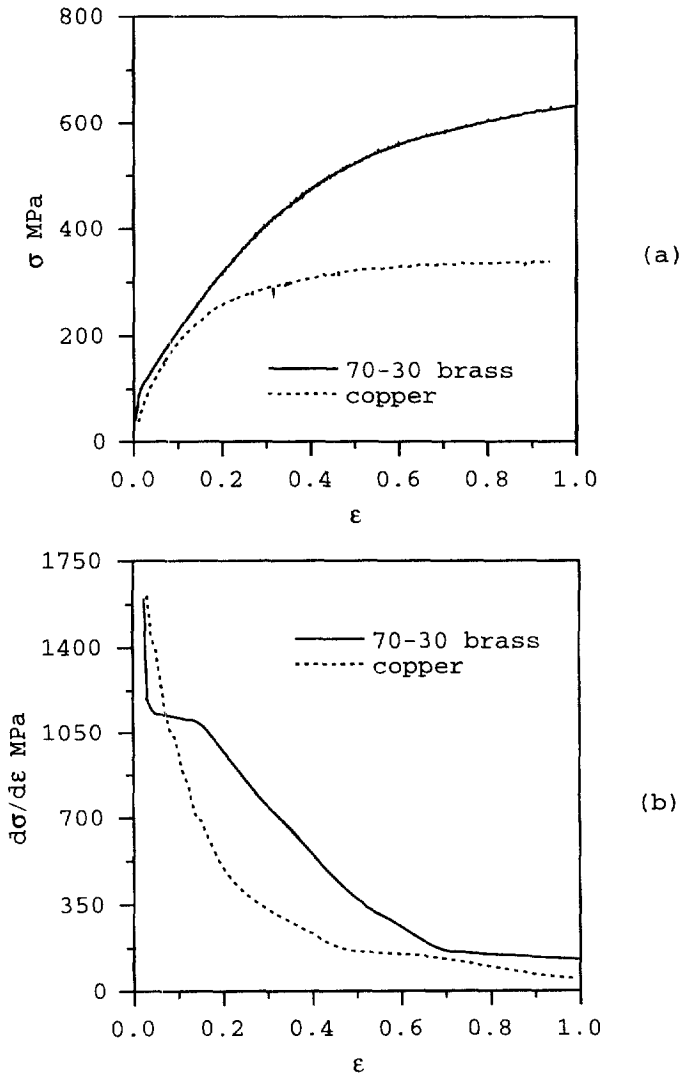


Fig. 2. (a) Stress-strain curves, and (b) rate of strain-hardening vs strain in plane strain compression for 70-30 brass and copper.

in a sense, it produces new grains. Van Houtte (1978) appears to have been the first to propose a simple tractable scheme for reorientation of grains due to twinning during simulation of texture development in a polycrystal. Recently, Tome *et al.* (1991) and Lebensohn and Tome (1994) have discussed some limitations of Van Houtte's proposal, and have proposed two new schemes of their own; however, their schemes are only applicable in the context of Taylor-type and self-consistent polycrystal models. In this paper we shall carry out finite-element modeling of polycrystalline aggregates deforming by slip and twinning, and we will explore the appli-

cability of Van Houtte's scheme in predicting the crystallographic texture of f.c.c. 70–30 brass. In these calculations each finite element represents a single grain, and the constitutive response is given through a single-crystal constitutive model. The results from such calculations satisfy both compatibility and equilibrium in the aggregate (in the “weak” finite-element sense).

We note that all previous attempts to model polycrystalline plasticity due to both slip and twinning have been for the rigid-plastic, non-hardening case, and have been limited to the Taylor [e.g. Van Houtte (1978)] or the “self-consistent” [e.g. Lebensohn and Tome (1994)] averaging schemes for polycrystalline materials. In this paper we present our formulation of an elastic–plastic model, which also attempts to capture the major features of strain hardening due to slip–twin interactions. We also examine the applicability of a Taylor-type model for polycrystals by comparing the results from such a model against results from our finite-element model of a polycrystal.

The plan of this paper is as follows. In Section 2 we set down a rate-independent constitutive model which accounts for both slip and twinning. Algorithmic details of a time-integration procedure, together with a new scheme to determine the active systems and the shear increments on the active slip and twin systems, are given in Appendix A. We have implemented our constitutive equations and computational procedures in the finite element program ABAQUS/Explicit (1995). This computational capability allows us to perform two types of finite element calculations: (i) where a finite element represents a single grain and the constitutive response is given through a single-crystal constitutive mode, and (ii) where a finite element quadrature point represents a material point in a polycrystalline sample and the constitutive response is given through a Taylor-type polycrystal model.

In Section 3 we use the former capability of our finite-element code to simulate the “nominally-homogeneous” deformations of plane-strain compression and simple compression of a polycrystalline aggregate, using a multitude of single crystals. Important ingredients in the theory are the slip and twin resistances, and their interaction and evolution. Direct measurements of the hardening interactions are difficult, if not impossible. Much work needs to be done to improve our understanding of these hardening interactions and their mathematical representation. In this context, Hirsch *et al.* (1988), Leffers and Bilde-Sorensen (1990), Leffers (1991), and Leffers and Jensen (1993) point out that in rolled brass $\{111\} \langle 11\bar{2} \rangle$ twins form as thin lamellae which are not homogeneously distributed, but cluster to form bundles in grains. These bundles are usually parallel to one plane of the $\{111\}$ family. Subsequent slip in grains containing such twin clusters occurs predominantly on $\{111\} \langle 110 \rangle$ slip systems with slip planes parallel to the plane of the twin bundles, and slip on other systems is restricted. Based on these experimental observations, we make plausible assumptions concerning the hardening part of the model, and use comparisons between model predictions and macroscopically-measured stress–strain curves and texture evolution to deduce information about the values of the single-crystal parameters associated with slip and twin system deformation resistances and hardening due to slip and twinning. We show that our model is able to reproduce both the experimentally-measured pole figures and the stress–strain curves in plane strain compression. Next, with the model so calibrated, we show that the predictions for the texture and stress–

strain curves from the model are also in reasonably good agreement with experiments in simple compression.

In Section 4 we evaluate the applicability of a Taylor-type model for combined slip and twinning. Our calculations show that for the high-symmetry f.c.c. brass, a Taylor-type model for crystals deforming by combined slip and twinning is able to predict reasonably well the macroscopic stress-strain curves and crystallographic texture evolution, in both plane-strain compression and simple compression. We close in Section 5 with some final remarks.

2. CONSTITUTIVE EQUATIONS

The overall plastic deformation of a crystal is always inhomogeneous at length scales associated with slip and twinning, and should be defined as an average over a volume element that must contain enough dislocation loops and twins to result in an acceptably smooth process at the continuum level of interest here. The smallest such volume element above which the plastic response can be considered smooth, is labeled as a representative-volume element. In our model, we will not account for the fine spatial structure of dislocation loops, slip bands and twin lamella in a crystal and we take a whole crystal as a representative-volume element. In particular, for later use, we denote the volume fraction of twins corresponding to the i th twin system by $f^i \geq 0$, with $\sum_i f^i \leq 1$. Also, we assume that there is no de-twinning and require that $\dot{f}^i \geq 0$.

The three major kinematic issues in modeling twinning are: (i) accounting for the shear associated with twinning; (ii) accounting for the reorientation of the crystal lattice due to twinning; and (iii) since splitting a grain and treating the twinned fractions as new orientations quickly lead to a numerically unmanageable number of grains, clever ways to handle twinning are needed. Van Houtte (1978) appears to have been the first to propose a simple tractable scheme for reorientation of grains due to twinning during simulation of texture development in a polycrystal. His scheme does not increase the number of crystals. In his approach, if a grain twins then the shear due to twinning is first accumulated as a pseudo-slip, that is, the shearing rate on the twin system is taken to be given by $\dot{\gamma}^i = \dot{f}^i \gamma_0$, where γ_0 is the amount of twinning shear, and the crystal lattice is given the twinning-related orientation only if a probabilistic criterion, based on the relative volume fractions of the twinned and non-twinned parts of a crystal, is met.

A constitutive model for deformation of a single crystal by combined slip and twinning will be developed by modifying the widely used framework for crystal plasticity by slip alone. The governing variables in the constitutive model are taken as: (i) The Cauchy stress, \mathbf{T} . (ii) The deformation gradient, \mathbf{F} . (iii) Crystal slip and twin systems labeled by integers i . Each system is specified by a unit normal \mathbf{n}_0^i to the slip/twin plane, and a unit vector \mathbf{m}_0^i denoting the slip/twin direction. The slip and twin systems $(\mathbf{m}_0^i, \mathbf{n}_0^i)$ are assumed to be known in the reference configuration. The amount of shear, γ_0 , and the lattice rotation accompanying twinning, \mathbf{R}^{tw} , are also assumed to be known. (iv) A plastic deformation gradient, \mathbf{F}^{p} , with $\det \mathbf{F}^{\text{p}} = 1$. This represents the cumulative effect of dislocation motion and shear due to twinning on

the active slip and twin systems in the crystal. (v) The slip and twin system deformation resistances $s^i > 0$, with units of stress. (vi) The twin fractions $f^i \geq 0$.

The elastic deformation gradient is defined by $\mathbf{F}^e \equiv \mathbf{F}\mathbf{F}^p^{-1}$ with $\det \mathbf{F}^e > 0$, and it describes the elastic distortion of the lattice; it is this distortion that gives rise to the stress \mathbf{T} .

Next, let $\bar{\mathbf{S}}_0 = (\det \mathbf{F})\mathbf{T}\mathbf{F}^{-T}$ denote the first Piola–Kirchhoff stress. Then, the stress power per unit reference volume is $\dot{\omega} = \bar{\mathbf{S}}_0 \cdot \dot{\mathbf{F}}$, which, since $\det \mathbf{F}^p = 1$, is also equal to the stress power per unit volume of the relaxed configuration determined by \mathbf{F}^p . This stress power may be additively decomposed as $\dot{\omega} = \dot{\omega}^e + \dot{\omega}^p$, where $\dot{\omega}^e = \mathbf{T}^* \cdot \dot{\mathbf{E}}^e$ is the elastic stress power per unit volume of the relaxed configuration, with

$$\mathbf{E}^e \equiv (1/2)\{\mathbf{F}^{eT}\mathbf{F}^e - \mathbf{1}\} \quad \text{and} \quad \mathbf{T}^* \equiv (\det \mathbf{F}^e)\mathbf{F}^{e-1}\mathbf{T}\mathbf{F}^{e-T} \quad (1)$$

the Green elastic strain measure and the symmetric second Piola–Kirchhoff stress tensor relative to the relaxed configuration, respectively, and

$$\dot{\omega}^p = (\mathbf{C}^e\mathbf{T}^*) \cdot (\dot{\mathbf{F}}^p\mathbf{F}^{p-1}), \quad \mathbf{C}^e \equiv \mathbf{F}^{eT}\mathbf{F}^e, \quad (2)$$

the plastic stress power per unit volume of the relaxed configuration.

Constitutive equation for stress

Elastic stretches in metallic single crystals are generally small. Accordingly, the constitutive equation for the stress in a metallic single crystal is taken as the linear relation

$$\mathbf{T}^* = \mathcal{C}[\mathbf{E}^e], \quad (3)$$

where \mathcal{C} is a fourth-order anisotropic elasticity tensor, where \mathbf{E}^e and \mathbf{T}^* are the strain and stress measures defined in eqn (1).

Slip and twinning conditions

Let

$$\mathbf{S}_0^i = \mathbf{m}_0^i \otimes \mathbf{n}_0^i \quad (4)$$

denote the Schmidt tensors, and consistent with eqn (2), let

$$\tau^i = (\mathbf{C}^e\mathbf{T}^*) \cdot \mathbf{S}_0^i \quad (5)$$

denote the resolved shear stress on the i th slip/twin system. Then, the conditions for slip and twinning are taken as

$$\phi^i = |\tau^i| - s^i = 0. \quad (6)$$

Flow rule

The evolution of the plastic deformation gradient is

$$\dot{\mathbf{F}}^p = \mathbf{L}^p\mathbf{F}^p, \quad (7)$$

with \mathbf{L}^p given by the sum of the shearing rates on all the slip and twin systems

$$\mathbf{L}^P = \sum_i \dot{\gamma}^i \text{sign}(\tau^i) \mathbf{S}_0^i. \quad (8)$$

The shearing rates are restricted as follows:

$$\dot{\gamma}^i \geq 0, \quad \text{and} \quad \dot{\gamma}^i \phi^i = 0. \quad (9)$$

Evolution equations for slip and twin resistances

These are generically taken as

$$\dot{s}^i = \sum_j h^{ij} \dot{\gamma}^j, \quad (10)$$

where h^{ij} are the hardening moduli. More on this later.

Consistency conditions

During plastic flow the following consistency conditions must be satisfied:

$$\dot{\gamma}^i \dot{\phi}^i = 0 \quad \text{if} \quad \phi^i = 0. \quad (11)$$

The consistency conditions serve to determine the shearing rates $\dot{\gamma}^i \geq 0$ on the slip and twin systems.

Evolution equations for twin volume fractions

For the twin systems,

$$\dot{f}^i = \dot{\gamma}^i / \gamma_0 \geq 0, \quad (12)$$

where γ_0 is the twinning shear.

Lattice reorientation condition

Let f denote the volume fraction of the twin system with the maximum value of f^i at a given time t , and let $\xi \in [0.2, 1]$ denote a random number. The lattice reorientation condition suggested by Van Houtte (1978), and adopted here, is that if $f > \xi$, then the orientation of the whole crystal be replaced by the twin related orientation. That is, if $\{\mathbf{e}_i^c \mid i = 1, 2, 3\}$ denotes a local orthonormal basis associated with the crystal lattice in the old relaxed configuration, then once this probabilistic criterion is met the crystal basis in the new relaxed configuration of the crystal be taken as $\mathbf{e}_i^{c*} = \mathbf{R}^{tw} \mathbf{e}_i^c$. To fix ideas, a schematic of the incremental kinematics of slip and twinning outlined above is shown in Fig. 3.

Further, if the lattice reorientation condition is met, then the twin volume fractions f^i are reinitialized to zero, and in our strain-hardening model we shall set all twin system deformation resistances to a value corresponding to that for the twin system with the maximum f^i prior to the reorientation. Also, the value of all slip system resistances are set equal to the value of the resistance for the slip system(s) parallel to the twin system with the maximum f^i prior to the reorientation.

A time-integration procedure for the constitutive equations is outlined in Appendix A. The constitutive equations and the time-integration procedure have been

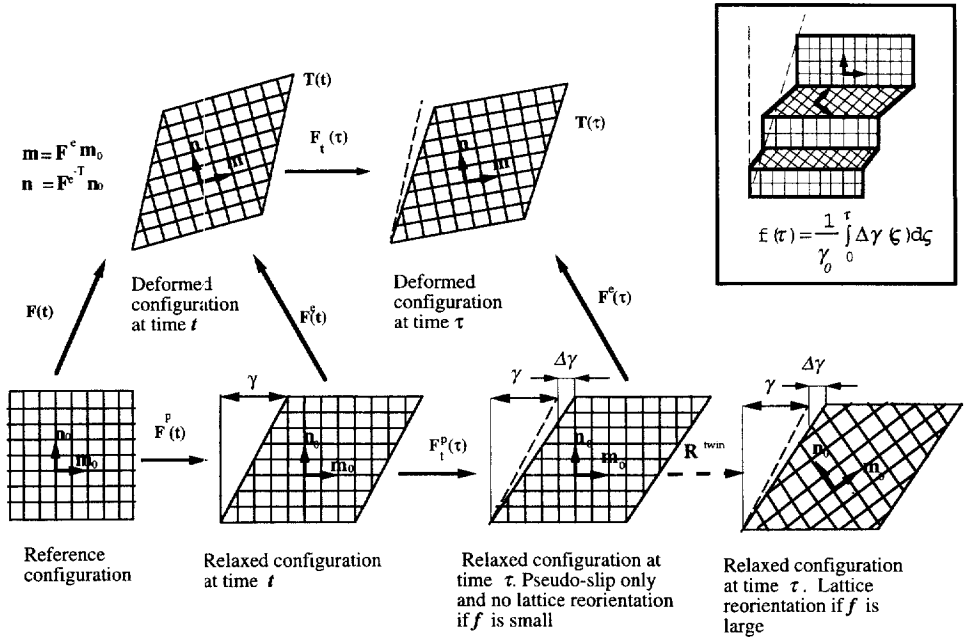


Fig. 3. Schematic of the incremental kinematics of slip and twinning.

implemented in the finite-element program ABAQUS/Explicit (1995) by writing a “user material” subroutine.

Our literature search has shown that all previous calculations of polycrystalline plasticity due to slip and twinning have been limited to the Taylor (Van Houtte, 1978), Sachs (Leffers, 1991), or self-consistent (Lebensohn and Tome, 1994) averaging schemes. These averaging schemes add another level of assumptions which may mask some of the consequences of the underlying features in our constitutive model for the response of a single crystal. To circumvent this difficulty the polycrystal calculations shown in the following section were carried out by modeling each crystal in a polycrystalline aggregate as a single finite element. In the finite-element model of a polycrystal, both compatibility and equilibrium conditions are satisfied; and there is no need for the Taylor, Sachs or any other hypotheses, which have been classically used to obtain the response of polycrystalline aggregates.

3. PLANE-STRAIN DEFORMATION OF F.C.C. 70-30 BRASS BY SLIP AND TWINNING

The elastic constants for brass single crystals are (Simmons and Wang, 1971):

$$C_{11} = 134 \text{ GPa}, \quad C_{12} = 105 \text{ GPa}, \quad C_{44} = 70 \text{ GPa}.$$

Table 1. *The twelve {111} <110> slip systems*

$[0\bar{1}\bar{1}]$	$\begin{matrix} (111) \\ [\bar{1}01] \end{matrix}$	$[1\bar{1}0]$	$[0\bar{1}\bar{1}]$	$\begin{matrix} (\bar{1}\bar{1}1) \\ [101] \end{matrix}$	$[\bar{1}10]$	$[01\bar{1}]$	$\begin{matrix} (\bar{1}11) \\ [101] \end{matrix}$	$[\bar{1}\bar{1}0]$	$[0\bar{1}\bar{1}]$	$\begin{matrix} (1\bar{1}1) \\ [\bar{1}01] \end{matrix}$	$[110]$
---------------------	--	---------------	---------------------	--	---------------	---------------	--	---------------------	---------------------	--	---------

Table 2. *The twelve {111} <112̄> twin systems*

$[\bar{2}11]$	$\begin{matrix} (111) \\ [1\bar{2}1] \end{matrix}$	$[11\bar{2}]$	$[2\bar{1}1]$	$\begin{matrix} (\bar{1}\bar{1}1) \\ [\bar{1}21] \end{matrix}$	$[\bar{1}\bar{1}\bar{2}]$	$[211]$	$\begin{matrix} (\bar{1}11) \\ [\bar{1}\bar{2}1] \end{matrix}$	$[\bar{1}1\bar{2}]$	$[\bar{2}\bar{1}1]$	$\begin{matrix} (1\bar{1}1) \\ [121] \end{matrix}$	$[1\bar{1}\bar{2}]$
---------------	--	---------------	---------------	--	---------------------------	---------	--	---------------------	---------------------	--	---------------------

Slip in f.c.c. crystals occurs on twelve {111} <110> slip systems listed in Table 1. Note that on a given slip system, slip can occur in either the positive or negative <110> slip direction in a {111} plane.

Twinning in f.c.c. crystals occurs on twelve {111} <112̄> twin systems are listed in Table 2 (e.g. Kelly and Groves, 1970). Note that unlike the slip systems listed in Table 1 for which slip can occur in either the positive or negative <110> slip direction in a {111} plane, twinning, because the underlying atomic arrangement is polar in nature, can occur in only one <112̄> type direction on a {111} plane, and the twin systems listed in Table 2 correspond to the easy direction of twinning. We do not consider the possibility of “de-twinning” in this paper.

The twinning shear corresponding to a twin system may be written as

$$\mathbf{1} + \gamma_0 \mathbf{m} \otimes \mathbf{n}, \quad \mathbf{m} \cdot \mathbf{n} = 0, \quad \gamma_0 = 1/\sqrt{2}, \tag{13}$$

where \mathbf{m} is a unit vector in a <112̄> direction, and \mathbf{n} the unit normal to the associated {111} plane. The corresponding twinning rotation is given by

$$\mathbf{R}^{tw} = 2\mathbf{n} \otimes \mathbf{n} - \mathbf{1}. \tag{14}$$

Henceforth, to distinguish the slip and twin resistances, we adopt the notation s^i and s^z to denote the slip and twin resistances, respectively. The initial values of these resistances are denoted by s_0^i and s_0^z .

Representation of the slip-twin hardening and hardening interactions is one of the major uncertainties, and much work needs to be done to improve our understanding of these hardening interactions and their mathematical representation. A simple phenomenological model for the evolution of s^i and s^z is formulated below.

During the “pseudo-slip” phase the twin system deformation resistances may be taken as constant, and the slip system deformation resistances are taken to evolve in the form [e.g. Kalidindi *et al.* (1992)]:

$$s^i = \sum_j h^{ij} \gamma^j, \quad \text{where} \quad h^{ij} = q^{ij} h^j. \tag{15}$$

Here h^{ij} are components of the hardening matrix,

$$q^{ij} = [q + (1 - q)\delta^{ij}] \quad (16)$$

is the matrix describing the latent hardening, with $q = 1.0$ for co-planar systems and $q = 1.4$ for non-coplanar systems,† and

$$h^i = h_0 \left(1 - \frac{s^i}{\bar{s}}\right)^a \quad (17)$$

is the single slip hardening rate, with $\{h_0, \bar{s}, a\}$ being the slip system hardening parameters, which are taken to be identical for all slip systems.

As mentioned previously, Leffers and co-workers (e.g. 1991, 1993) have reported that during plane strain compression of brass, twins form thin lamellae which cluster to form bundles in grains, and that subsequent slip is restricted to planes which are parallel to these twin bundles. We have modeled this kinematic restriction on the activity of the slip systems as follows. When the fraction $f = \max\{f^\alpha\}$, the maximum value of f^α taken over all twin systems, reaches a value λ (between 3–5%), slipping and twinning in systems whose slip/twin planes are not parallel to the plane of the twin system with maximum f^α are restricted by choosing appropriate values of slip and twin resistances. Let \mathcal{T}_λ denote the single element set denoting the twin system for which f^α reaches the value λ , with corresponding resistance $s_{tw,\lambda}$. Also, let \mathcal{S}_λ denote the set of slip systems which are parallel to this twin system. Then the evolution of $s_{tw,\lambda}$ may be taken in the saturation form

$$\dot{s}_{tw,\lambda}(\tau) = h_{tw}\dot{\gamma}_{tw}, \quad \text{with} \quad h_{tw} = h_0^{tw} \left(1 - \frac{s_{tw,\lambda}}{\bar{s}_{tw}}\right)^{a_{tw}}, \quad (18)$$

where $\dot{\gamma}_{tw}$ is the shearing rate due to twinning in the major twin system, and h_0^{tw} , \bar{s}_{tw} , and a_{tw} are constants for a particular material. Also, for the other twinning systems, setting

$$s^\alpha = 5 \times s_0^\alpha, \quad \text{for } \alpha \notin \mathcal{T}_\lambda, \quad (19)$$

renders them inoperative. For the slip systems co-planar with the major twin system, requiring

$$s^i \leq s_{tw,\lambda}, \quad \text{for } i \in \mathcal{S}_\lambda,$$

keeps them operative. Also, since twin lamellae are serious obstacles to dislocation glide they cause additional hardening of the slip systems not in \mathcal{S}_λ . A simple phenomenological form for this hardening interaction is as follows:

$$\dot{s}^i = \sum_j h^{ij}\dot{\gamma}^j + h_{tw-sl}^i \dot{\gamma}^{tw}, \quad \text{for } i \notin \mathcal{S}_\lambda, \quad (20)$$

where $\dot{\gamma}_{tw}$ is the shearing rate due to twinning in the major twin system, and the last term represents twin-slip hardening. A simple saturation-type form for the twin-slip hardening rate is

† We recognize that this is a greatly simplified description of latent hardening. However, our numerical experiments show that the macroscopic stress-strain curves and crystallographic texture evolution are not significantly altered when we change the values of q .

$$h_{\text{tw-sl}}^i = h_0^{\text{tw-sl}} \left(1 - \frac{s^i}{\tilde{s}_{\text{tw-sl}}} \right)^{a_{\text{tw-sl}}}, \quad (21)$$

where $h_0^{\text{tw-sl}}$, $\tilde{s}_{\text{tw-sl}}$, and $a_{\text{tw-sl}}$ are additional material constants.

To summarize, the parameters s_0^i , s_0^z denote the initial values of the slip and twin resistances; the hardening parameters $\{h_0, \tilde{s}, a\}$ are associated with slip hardening during the pseudo-slip phase; the hardening parameters $\{h_0^{\text{tw}}, \tilde{s}_{\text{tw}}, a_{\text{tw}}\}$ are associated with the self-hardening of the major twin system; and the parameters $\{h_0^{\text{tw-sl}}, \tilde{s}_{\text{tw-sl}}, a_{\text{tw-sl}}\}$ are associated with the enhanced hardening due to the interaction of the dominant twin system with the slip systems not parallel to it. These parameters are obtained by judiciously adjusting their values so that the model reproduces the plane strain compression stress-strain curve obtained from experiments on 70-30 brass.

As-received 70-30 brass was annealed at 600°C for one hour in an inert atmosphere. Plane strain experiments were conducted at room temperature and at a quasi-static strain rate of 0.006 s⁻¹. The dimensions of the plane strain compression specimens were 12.7 mm in the compression direction, 10 mm in the constrained direction, and 11 mm in the free direction. The specimens were lubricated with MoS₂ lubricant and teflon film to reduce friction. The stress-strain curve obtained from these experiments is shown in Fig. 4.

Finite-element calculations for plane strain compression of an aggregate of 343 initially randomly-oriented grains were carried out with various values of the material

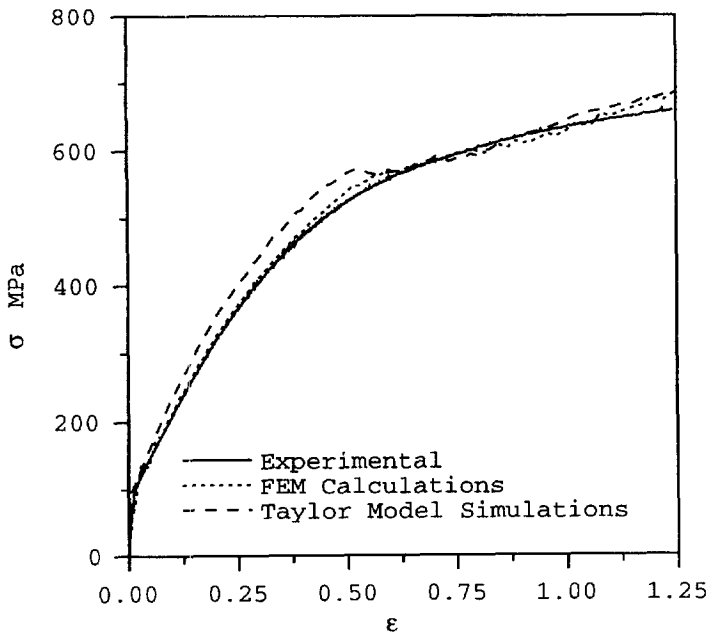
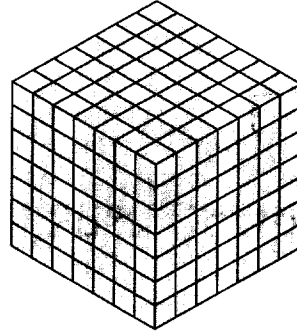


Fig. 4. Comparison of the experimentally-measured stress-strain curves for plain strain compression of α -brass against a finite-element model of a polycrystal, as well as against a Taylor model.



(a) Initial mesh

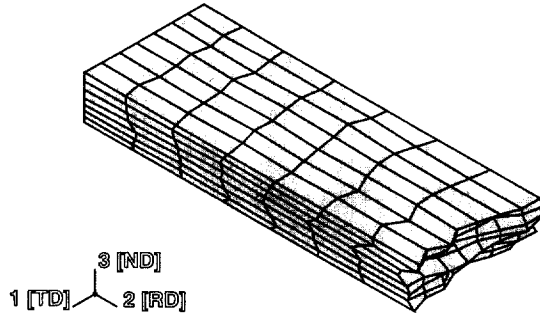


Fig. 5. Representative (a) initial, and (b) deformed 3-D finite-element meshes for plane strain compression.

parameters. Figure 5(a) shows the initial finite-element. The planes corresponding to $x_1 = 0$, $x_2 = 0$, and $x_3 = 0$ are confined such that all the nodes on these faces have zero u_1 , u_2 , and u_3 displacements, respectively. The displacement for the outer face of the specimen in the x_1 direction is set to $u_1 = 0$; the outer face in the x_2 direction has zero tractions, while a negative u_3 displacement is applied on the outside x_3 -face of the specimen. The process of curve-fitting the plane strain compression stress-strain data to obtain the value of the hardening parameters yields

$$s_0^i = 25 \text{ MPa}, \quad s_0^z = 155 \text{ MPa},$$

$$h_0 = 135 \text{ MPa}, \quad \bar{s} = 400 \text{ MPa}, \quad a = 2,$$

$$h_0^{\text{tw}} = 452 \text{ MPa}, \quad \bar{s}_{\text{tw}} = 245 \text{ MPa}, \quad a_{\text{tw}} = 0.25,$$

and

$$h_0^{\text{tw-sl}} = 1.06 \text{ GPa}, \quad \bar{s}_{\text{tw-sl}} = 245 \text{ MPa}, \quad a_{\text{tw-sl}} = 0.25.$$

The quality of the curve-fit is shown in Fig. 4. One can see that the calculated stress-strain response is very close to the experimentally observed one. The jumps on the

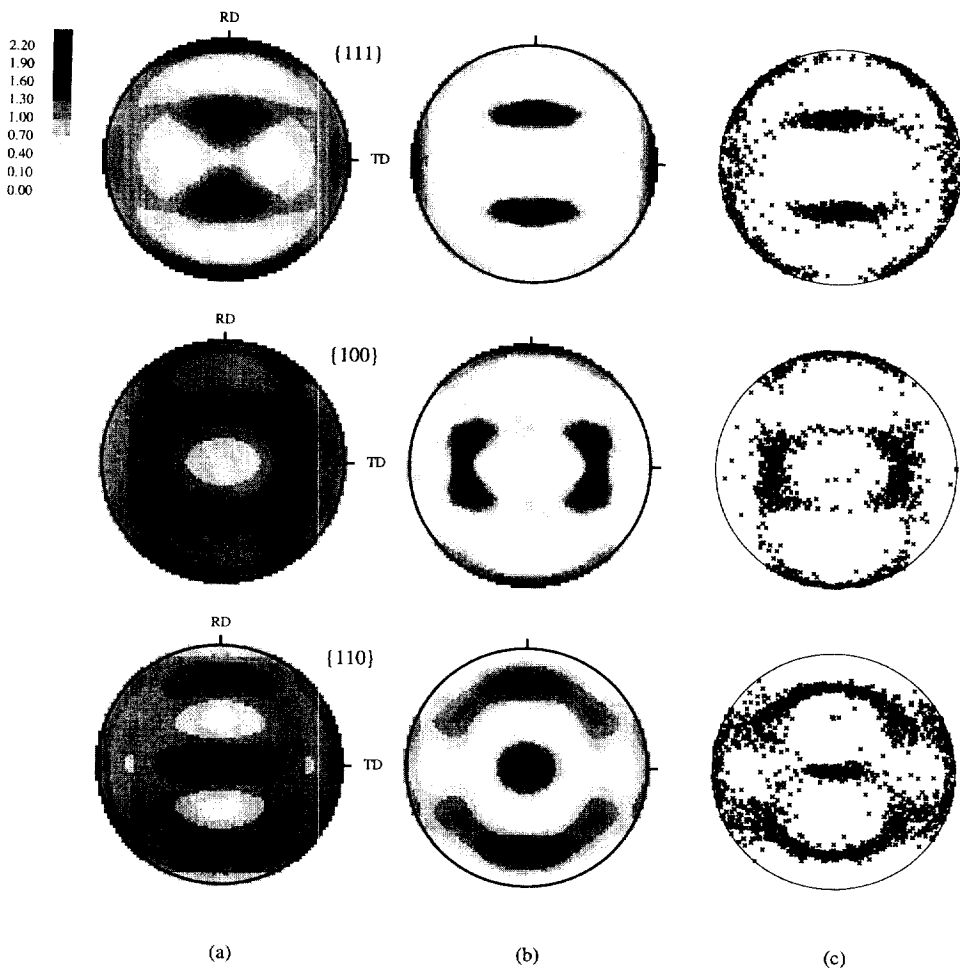


Fig. 6. Comparison of experimentally-measured pole-figures after 100% plane strain compression of α -brass against predictions from numerical simulations. (a) Experimental results. (b) The discrete predictions from finite-element calculations shown in (c) are smoothed to show grey-scale intensities using popLA.

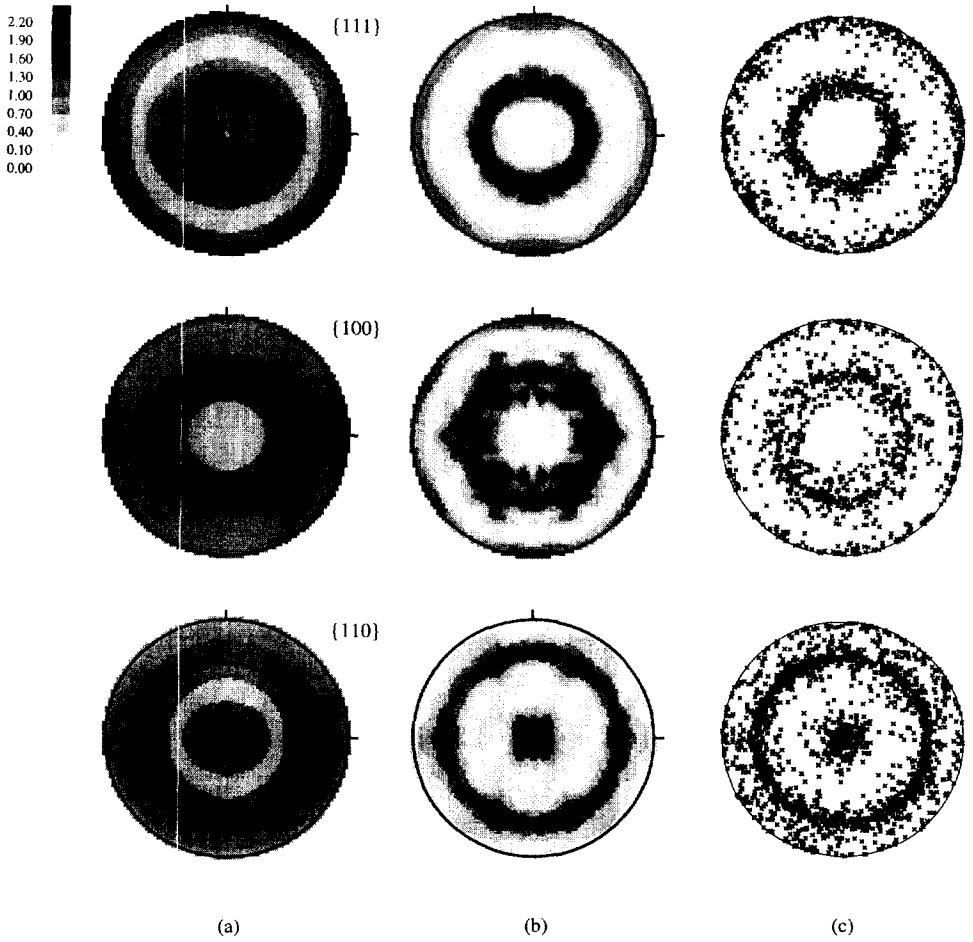


Fig. 8. Comparison of experimentally-measured pole-figures after 100% simple compression of α -brass against predictions from numerical simulations. (a) Experimental results. (b) The discrete predictions from finite-element calculations shown in (c) are smoothed to show grey-scale intensities using popLA.

numerically calculated curve at strains greater than ≈ 0.5 are due to the crystal lattice rotations of the grains during twinning.†

Experimental measurements of texture of the samples after deformation were carried out by X-ray irradiation, using a Rigaku RU200 diffractometer. Pole figures were obtained by using the Shultz reflection method with copper- K_α radiation. To process the experimental data, the Preferred Orientation Package [Kallend *et al.* (1991)] was employed. Each measured pole figure was corrected for background and defocusing, and also extrapolated for the outer 15° . The $\{111\}$, $\{100\}$, and $\{110\}$ pole figures for plane strain compression after 100% compression are shown in Fig. 6; all pole figures are equal-area projections of the specified crystallographic planes. This figure also shows the numerically-predicted pole figures. The agreement between the numerical prediction and experimental measurements, especially for the $\{111\}$ and $\{100\}$ pole figures, is very good.

The numerical calculations show that because of the different values of $s_0^i = 25$ MPa and $s_0^z = 155$ MPa, in the initial stages of deformation the grains deform by crystallographic slip only. The slip deformation resistances increase due to strain-hardening, and at a level of macroscopic strain of approximately 10–15%, the first threshold, $\lambda = 0.04$, for the twin fraction $f = \max\{f^z\}$ used to restrict slip, is reached in some grains. At this stage the resistances for twinning on all systems other than the twin system with maximum value of f^z were set to values five times their initial values, and our choice of hardening parameters ensures that the slip resistances increase very fast for all systems other than those which are co-planar with the dominant twin system; dominant crystallographic shearing occurs along the chosen crystallographic plane in a given crystal. When the second threshold for the twin fraction $f = \max\{f^z\}$ is reached, $f > \xi$, $\xi \in [0.2, 1]$, with ξ a random number, the crystal lattice is replaced with a twin-related one, and as discussed previously, all twin system deformation resistances and all slip system resistances are set to the values corresponding to those for the active twin system. With our choice of material parameters, the crystal lattice rotation due to twinning starts at about 45% macroscopic strain. Before this level of deformation, the calculated pole figures are very close to those typical for f.c.c. materials deforming by slip alone. In our model twinning affects the predicted texture of the material in two ways: (i) restriction of slip to slip planes parallel to the dominant twin system in a grain; and (ii) reorientation of the lattice of grains to the twin-related orientations. Numerical results (not reported here) show that the first mechanism alone is insufficient to produce the distinguishing “brass-type” texture. Our numerical experimentation shows that the “brass-texture” is a result of both constrained slip, and the lattice reorientation due to twinning.

The set of material parameters fit to the plane strain compression data has also been used to predict the response in simple compression. For the simple compression experiments, cylindrical specimens with an initial ratio between height and diameter of 1.5 were used. Figure 7 shows that numerically-predicted stress–strain response is close to the experimentally measured one. Figure 8 shows the measured and predicted pole figures at a strain of 100%. The agreement is very good.

† Comparison of the predicted stress–strain curves using 100 elements rather than 343 elements shows that the curves are smoother when a larger number of elements are used in the polycrystal model simulation.

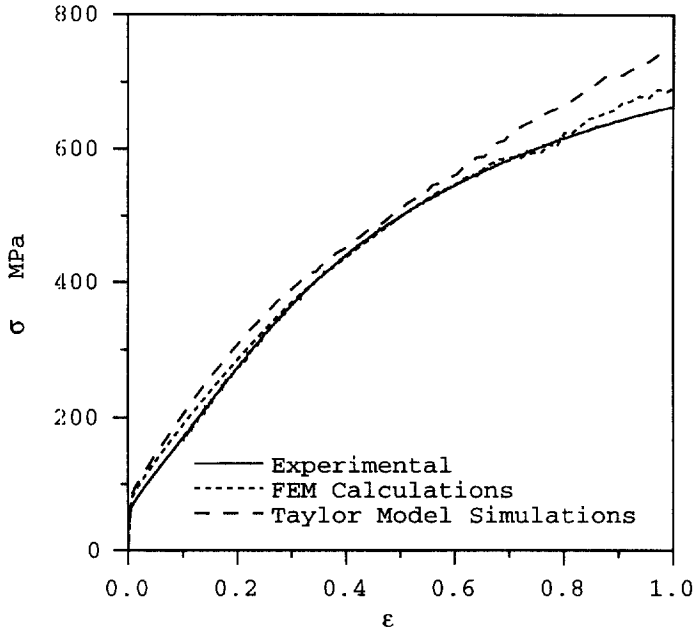


Fig. 7. Comparison of the experimentally-measured stress-strain curves for simple compression of α -brass against a finite element model of a polycrystal, as well as against a Taylor model.

4. TAYLOR-MODEL SIMULATIONS

A very large body of literature exists on application of the Taylor model for texture prediction. The main assumption of this model for a polycrystal is that the deformation gradient in each grain is homogeneous and equal to the macroscopic one at a material point. The compatibility condition is automatically satisfied in this approximation; however, equilibrium holds only inside a grain, but is violated between grains. If, in addition, we assume that all grains have equal volume, then the average Cauchy stress at each macroscopic continuum point is simply the number-averaged stress (Taylor, 1938a, b; Asaro and Needleman, 1985):

$$\mathbf{T} = \frac{1}{N} \sum_{k=1}^{k=N} \mathbf{T}^k, \quad (22)$$

where \mathbf{T}^k is the Cauchy stress in the k -th crystal, and N is the total number of crystals comprising the material point.

By comparing the Taylor model predicted stress-strain responses and crystallographic textures against results from FEM simulations, Bronkhorst *et al.* (1992) showed that a Taylor-type model of a polycrystal provides an acceptable description of the behavior of single-phase f.c.c. polycrystals deforming by slip alone. We have employed the same method to check on the applicability of a Taylor model for combined slip and twinning. With the material parameters calibrated for the finite-

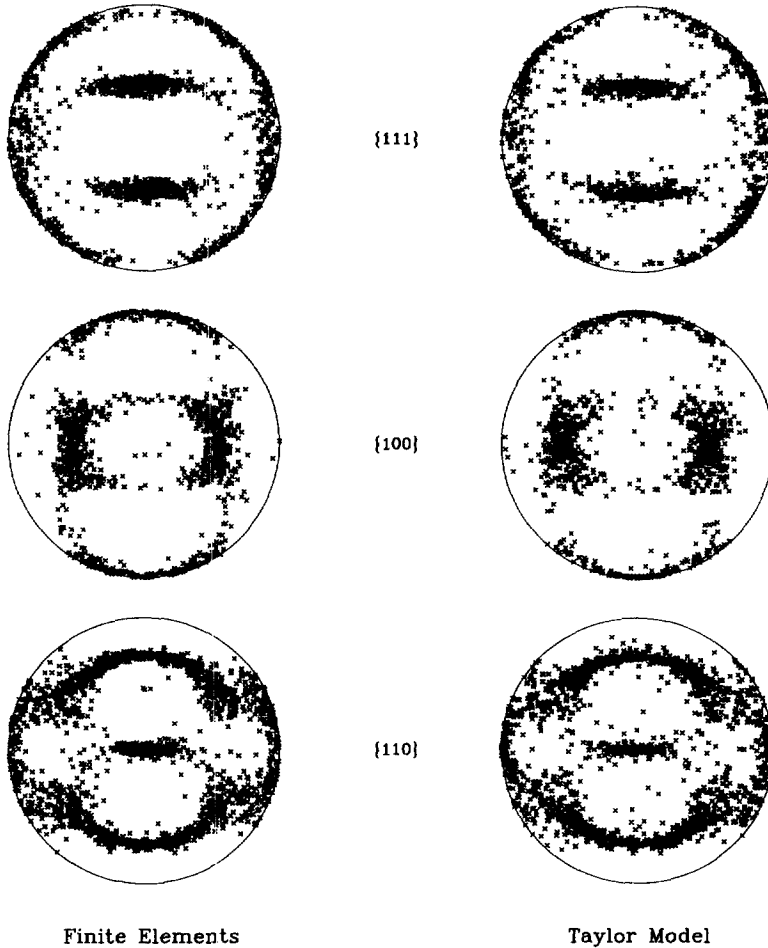


Fig. 9. Comparison of the pole-figures after 100% plane strain compression predicted from a finite-element model of a polycrystal against those predicted by a Taylor model.

element model of the polycrystal, our Taylor model simulations slightly overpredict the stress-strain responses in both plane strain compression and simple compression, Figs 4 and 7, respectively. Figures 9 and 10 show the predictions for the crystallographic texture, using both the finite-element model and the Taylor model for plane strain compression and simple compression, respectively. The texture predictions from the two modeling schemes are very similar. Thus, as for f.c.c. materials which deform by slip alone, the Taylor model may also be used for obtaining computationally inexpensive and reasonably accurate predictions of both the stress-strain curve and the crystallographic texture of f.c.c. materials deforming by combined slip and twinning.

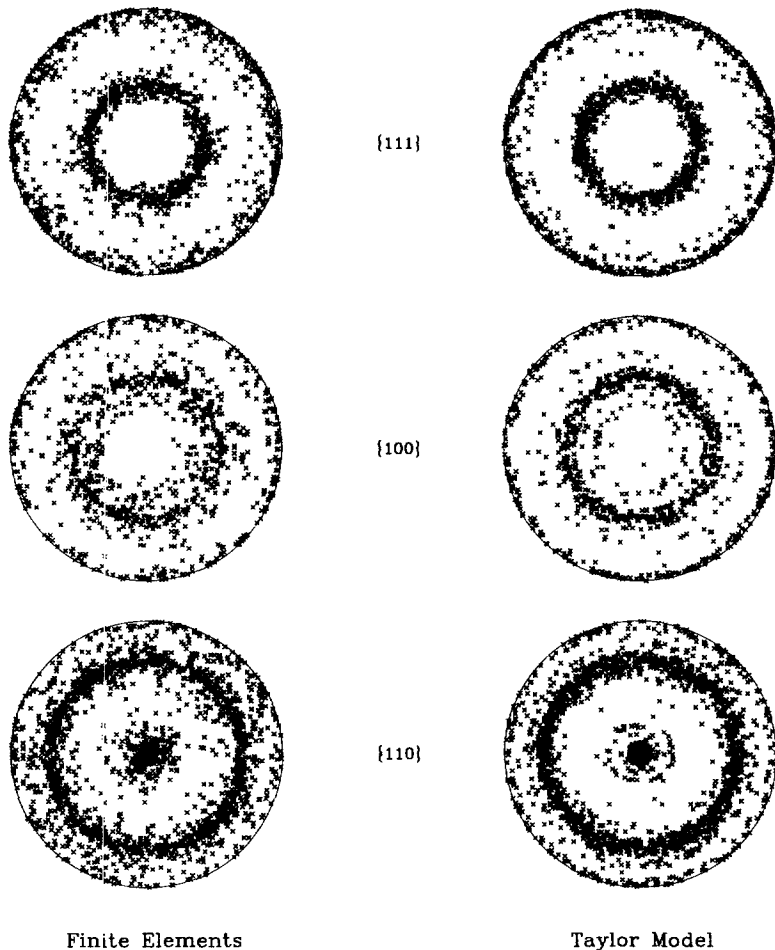


Fig. 10. Comparison of the pole-figures after 100% simple compression predicted from a finite-element model of a polycrystal against those predicted by a Taylor model.

5. CONCLUDING REMARKS

To summarize, a rate-independent, elastic-plastic, constitutive model for plastic deformation of f.c.c. polycrystalline materials deforming by both slip and twinning has been developed. The model has been implemented in the finite-element program ABAQUS/Explicit (1995).

Full finite-element models of a polycrystal (in which both compatibility and equilibrium are satisfied) are used to carry out plane strain compression simulations. By using comparisons between model predictions and macroscopically-measured stress-strain curves on 70-30 brass, we have deduced information about the values of the single-crystal parameters associated with slip and twin system deformation resistances and hardening due to slip and twinning. The predicted crystallographic texture from

the finite-element calculations is in good accord with experiments. The simulation capability also successfully predicts the stress-strain response and crystallographic texture evolution in simple compression experiments.

We have also evaluated the applicability of a simple Taylor-type model for combined slip and twinning. Our experiments and calculations show that, for the high-symmetry f.c.c. brass, a Taylor model for a polycrystal deforming by combined slip and twinning is able to predict reasonably well the macroscopic stress-strain curves and crystallographic texture evolution in both plane strain and simple compression.

ACKNOWLEDGEMENTS

The contributions of S. Balasubramanian and M. Kothari are gratefully acknowledged. The support for this work was provided by the U.S. Army Research Office under Grant DAAH04-94-G-0060, and the National Science Foundation under Grant CMS-9610130. The ABAQUS finite-element software was made available under an academic license from HKS, Inc., Pawtucket, R.I.

REFERENCES

- ABAQUS (1995) *Reference Manuals*. Hibbit, Karlsson and Sorensen Inc., Pawtucket, R.I.
- Anand, L. and Kalidindi, S. R. (1994) The process of shear band formation in plane strain compression of f.c.c. metals: effects of crystallographic texture. *Mechanics of Materials* **17**, 223–243.
- Anand, L. and Kothari, M. (1996) A computational procedure for rate-independent plasticity. *Journal of the Mechanics and Physics of Solids* **44**, 525–558.
- Asaro, R. J. and Needleman, A. (1985) Texture development and strain hardening in rate dependent polycrystals. *Acta Metallurgica* **33**, 923–953.
- Asgari, S., Kalidindi, S. and Doherty, R. D. (1997) Strain hardening and microstructural evolution during large strain compression of low stacking fault energy f.c.c. alloys that form deformation twins. *Metallurgical Transactions*, submitted.
- Balasubramanian, S. and Anand, L. (1996) Single crystal and polycrystal elasto-viscoplasticity: application to earing in cup drawing of f.c.c. materials. *Computational Mechanics* **17**, 209–225.
- Beaudoin, A. J., Dawson, P. R., Mathur, K. K., Kocks, U. F. and Korzekwa, D. A. (1994) Application of polycrystalline plasticity to sheet forming. *Computer Methods in Applied Mechanics and Engineering* **117**, 49–70.
- Bronkhorst, C. A., Kalidindi, S. R. and Anand, L. (1992) Polycrystal plasticity and the evolution of crystallographic texture in f.c.c. metals. *Philosophical Transactions of the Royal Society London A* **341**, 443–477.
- Chin, G. Y., Hosford, W. F. and Mendorf, D. R. (1969) Accommodation of constrained deformation in f.c.c. metals by slip and twinning. *Proceedings of the Royal Society A* **309**, 433–456.
- Chin, G. Y. and Mammel, W. L. (1969) Generalization and equivalence of the minimum work (Taylor) and maximum work (Bishop–Hill) principles of crystal plasticity. *Transactions of AIME* **245**, 1211–1214.
- Chin, G. Y. (1975) Development of deformation textures. In *Constitutive Equations in Plasticity*, ed. A. S. Argon, pp. 431–447.
- Dillamore, I. L. and Roberts, W. T. (1964) Rolling textures in f.c.c. and b.c.c. metals. *Acta Metallurgica* **12**, 281–293.

- Fletcher, R. and Powell, M. J. (1963) A rapidly convergent descent method for minimization. *Computer Journal* **6**, 163–168.
- Fletcher, R. and Reeves, C. M. (1964) Function minimization by conjugate gradients. *Computer Journal* **7**(2), 149–154.
- Goodman, S. R. and Hu, H. (1968) Texture development in copper and 70–30 brass. *Transactions of the Metallurgical Society of AIME* **242**, 88–93.
- Hirsch, J., Luke, K. and Hatherly, M. (1988) Mechanism of deformation and development of rolling textures in polycrystalline f.c.c. metals (Part III). *Acta Metallurgica* **36**(11), 2905–2927.
- Kalidindi, S. R., Bronkhorst, C. A. and Anand, L. (1992) Crystallographic texture evolution during bulk deformation processing of f.c.c. metals. *Journal of the Mechanics and Physics of Solids* **40**, 537–569.
- Kallend, J. S., Kocks, U. F., Rollett, A. D. and Wenk, H. R. (1991) *popLA: The Preferred Orientation Package from Los Alamos*. Los Alamos National Laboratory.
- Kelly, A. and Groves, G. W. (1970) *Crystallography and Crystal Defects*. Longman, London, pp. 290–312.
- Lebensohn, R. A. and Tome, C. N. (1994) A self-consistent viscoplastic model: prediction of rolling textures of anisotropic polycrystals. *Materials Science and Engineering* **A175**, 71–82.
- Leffers, T. (1991) Microstructures, textures, and deformation patterns at large strain. In *MECAMAT'91*. Balkema, Rotterdam, pp. 73–86.
- Leffers, T. and Bilde-Sorensen, J. B. (1990) Intra- and intergranular heterogeneities in plastic deformation of brass during rolling. *Acta Metallurgica et Materialia* **38**, 1917–1926.
- Leffers, T. and Jensen, D. J. (1993) In *Textures and Microstructures* **14–18**, 933–952.
- Mathur, K. K. and Dawson, P. R. (1989) On modeling and development of crystallographic texture in bulk forming processes. *International Journal of Plasticity* **5**, 67–94.
- Mathur, K. K. and Dawson, P. R. (1990) Texture development during wire drawing. *ASME Journal of Engineering Materials and Technology* **112**, 292–297.
- Press, W. H., Flannery, B. P., Teukolsky, S. A. and Vetterling, W. T. (1986) *Numerical Recipes: The Art of Scientific Computing*. Cambridge University Press, Cambridge, U.K.
- Simmons, G. and Wang, H. (1971) *Single Crystal Elastic Properties and Calculated Aggregate Properties: A HANDBOOK*. The MIT Press, Cambridge, U.S.A.
- Smallman, R. E. and Green, D. (1964) The dependence of rolling texture on stacking fault energy. *Acta Metallurgica* **12**, 145–154.
- Taylor, G. I. (1938a) Plastic strain in metals. *Journal of the Institute of Metals* **62**, 307–324.
- Taylor, G. I. (1938b) Analysis of plastic strain in a cubic crystal. *Stephen Timoshenko 60th Anniversary Volume*. MacMillan Co., New York, pp. 218–224.
- Tome, C. N., Lebensohn, R. A. and Kocks, U. F. (1991) A model for texture development dominated by deformation twinning: application to zirconium alloys. *Acta Metallurgica et Materialia* **39**, 2667–2680.
- Van Houtte, P. (1978) Simulation of the rolling and shear texture of brass by the Taylor theory adapted for mechanical twinning. *Acta Metallurgica* **26**, 591–604.
- Venables, J. A. (1964) The nucleation and propagation of deformation twins. *Journal of the Physics and Chemistry of Solids* **25**, 693–700.
- Wasserman, G. (1963) Der einfluss mechanischer zwillingsbildung auf die entstehung der walz-texturen kubisch flächenzentrierter metalle. *Zeitschrift für Metallkunde* **54**, 61–65.

APPENDIX A

Here we summarize a simple time-integration procedure for our rate-independent single crystal constitutive model. With t denoting the current time, Δt is an infinitesimal time increment, and $\tau = t + \Delta t$. The algorithm is as follows:

Given: (1) $\{\mathbf{F}(t), \mathbf{F}(\tau)\}$; (2) $\{\mathbf{T}(t), \mathbf{F}^p(t)\}$; (3) a rotation tensor $\bar{\mathbf{Q}}(t)$, which brings an orthonormal basis $\{\mathbf{e}_i^{(0)}(t)\}$ associated with the crystal to be in correspondence with a fixed orthonormal

basis $\{\mathbf{e}_i^{(g)}\}$ in space; (4) $\{\mathbf{m}_0^i(t), \mathbf{n}_0^i(t), s^i(t)\}$; and (5) the accumulated shears due to twinning $\Gamma^i(t)$, where the index i ranges over the previously active twin systems since the last reorientation of the lattice.

Calculate: (a) $\{\mathbf{T}(\tau), \mathbf{F}^p(\tau)\}$; (b) the accumulated shears due to twinning $\Gamma^i(\tau)$, where the index i ranges over the previously active twin systems since the last reorientation of the lattice; (c) the rotation tensor $\mathbf{Q}(\tau)$, which brings the orthonormal crystal basis $\{\mathbf{e}_i^{(g)}(\tau)\}$ to be in correspondence with a fixed orthonormal basis $\{\mathbf{e}_i^{(g)}\}$ in space; (d) $\{\mathbf{m}_0^i(\tau), \mathbf{n}_0^i(\tau), s^i(\tau)\}$; and (e) the orientation of the slip and systems in the deformed configuration at time τ from

$$\mathbf{m}_\tau^i = \mathbf{F}^e(\tau)\mathbf{m}_0^i(\tau), \quad \mathbf{n}_\tau^i = \mathbf{F}^e(\tau)^{-T}\mathbf{n}_0^i(\tau).$$

The steps used in the calculation procedure are:

Step 1. Calculate a trial elastic strain $\mathbf{E}^e(\tau)^{tr}$:

$$\begin{aligned} \mathbf{F}^e(\tau)^{tr} &= \mathbf{F}(\tau)\mathbf{F}^p(t)^{-1}, \\ \mathbf{C}^e(\tau)^{tr} &= (\mathbf{F}^e(\tau)^{tr})^T\mathbf{F}^e(\tau)^{tr}, \\ \mathbf{E}^e(\tau)^{tr} &= (1/2)\{\mathbf{C}^e(\tau)^{tr} - \mathbf{1}\}. \end{aligned}$$

Step 2. Calculate a trial stress $\mathbf{T}^*(\tau)^{tr}$:

$$\mathbf{T}^*(\tau)^{tr} = \mathcal{C}[\mathbf{E}^e(\tau)^{tr}].$$

Step 3. Calculate a trial resolved shear stress $\tau^i(\tau)^{tr}$ on each slip and twin system. Recall that the resolved shear stress was defined as $\tau(\tau) = \{\mathbf{C}^e(\tau)\mathbf{T}^*(\tau)\} \cdot \mathbf{S}_0(t)$, where $\mathbf{S}_0(t) = \mathbf{m}_0(t) \otimes \mathbf{n}_0(t)$. For infinitesimal elastic stretches the resolved shear stress $\tau(\tau)$ may be approximated at $\tau(\tau) \doteq \mathbf{T}^*(\tau) \cdot \mathbf{S}_0(t)$. Accordingly, the trial resolved shear stress is calculated as

$$\tau^i(\tau)^{tr} = \mathbf{T}^*(\tau)^{tr} \cdot \mathbf{S}_0^i(t).$$

Step 4. Determine the set $\mathcal{P}\mathcal{A}$ of potentially active slip and twin systems which satisfy

$$|\tau^i(\tau)^{tr}| - s^i(t) > 0.$$

Step 5. We shall use the following incremental versions of the flow rule and the evolution equations for the slip and twin systems resistances:

$$\begin{aligned} \mathbf{F}^p(\tau) &= \left\{ \mathbf{1} + \sum_{i \in \mathcal{P}\mathcal{A}} \Delta\gamma^i \text{sign}(\tau^i(\tau)^{tr}) \mathbf{S}_0^i(t) \right\} \mathbf{F}^p(t) \\ s^i(\tau) &= s^i(t) + \sum_{j \in \mathcal{P}\mathcal{A}} h^{ij}(t) \Delta\gamma^j, \quad i = 1, \dots, N, \end{aligned} \quad (23)$$

where N is the total number of slip and twin systems.

During plastic flow the active systems must satisfy the consistency condition

$$|\tau^i(\tau)| = s^i(\tau). \quad (24)$$

A calculation for $|\tau^i(\tau)|$, retaining terms of first order in $\Delta\gamma^j$, gives

$$|\tau^i(\tau)| = |\tau^i(\tau)^{tr}| - \sum_{j \in \mathcal{P}\mathcal{A}} \{\text{sign}(\tau^i(\tau)^{tr}) \text{sign}(\tau^j(\tau)^{tr}) \mathbf{S}_0^i(t) \cdot \mathcal{C}[\text{sym}(\mathcal{C}^e(\tau)^{tr} \mathbf{S}_0^j(t))]\} \Delta\gamma^j. \quad (25)$$

Use of eqns (23) and (25) in the consistency condition (24) gives

$$\sum_{j \in \mathcal{P}\mathcal{A}} A^{ij} x^j = b^i, \quad i \in \mathcal{P}\mathcal{A}, \quad (26)$$

with

$$A^{ij} = h^{ij} + \text{sign}(\tau^i(\tau)^{\text{tr}}) \text{sign}(\tau^j(\tau)^{\text{tr}}) \mathbf{S}_0^i(t) \cdot \mathcal{C}[\text{sym}(\mathcal{C}^e(\tau)^{\text{tr}} \mathbf{S}_0^i(t))], \quad (27)$$

$$b^i = |\tau^i(\tau)^{\text{tr}}| - s^i(t) > 0, \quad (28)$$

$$x^i \equiv \Delta\gamma^i \geq 0. \quad (29)$$

Equation (26) is a system of linear equations for $x^i \equiv \Delta\gamma^i \geq 0$, with the matrix A possibly singular.

For the case of slip alone, Anand and Kothari (1996) have recently proposed an iterative solution procedure based on the Singular Value Decomposition (SVD) of A to determine the active slip systems and the corresponding shear increments. In their procedure the shear increments are calculated as

$$x^+ = A^+ b,$$

where A^+ is the pseudo-inverse of the matrix of the matrix A , defined over all the potentially active slip and twin systems. If A is singular, then from the set of non-unique solutions to $Ax = b$, the chosen solution is the one which has the minimum length $\|x\|_2$. If for any system the solution $x^i = \Delta\gamma^i \leq 0$, then this system is inactive, and it is removed from the set of potentially active systems. The reduced system $Ax = b$ is solved again using the pseudo-inverse of the new A . This iterative procedure is continued until all $x^i = \Delta\gamma^i > 0$.

An alternate procedure which does not involve iterations, and which is based on a constrained quadratic minimization statement of the problem, is given in Appendix B. The solutions obtained by either method are identical. While the iterative method of Anand and Kothari is based on a robust implementation of the SVD of A (Press *et al.*, 1986), the method described in Appendix B is based on a conjugate gradient method to solve the minimization problem, and it has yet to be optimized. Accordingly, there is (as of now) no major increase in speed in obtaining the solution by the alternate method outlined in Appendix B.

Step 6. Update the plastic deformation gradient $\mathbf{F}^p(\tau)$:

$$\mathbf{F}^p(\tau) = \left\{ \mathbf{1} + \sum_{i \in \mathcal{A}} \text{sign}(\tau^i(\tau)^{\text{tr}}) \Delta\gamma^i \mathbf{S}_0^i(t) \right\} \mathbf{F}^p(t).$$

Step 7. Check if $\det \mathbf{F}^p(\tau) = 1$. If not, normalize $\mathbf{F}^p(\tau)$ as:

$$\mathbf{F}^p(\tau) = [\det \mathbf{F}^p(\tau)]^{-1/3} \mathbf{F}^p(\tau).$$

Step 8. Compute the elastic deformation gradient $\mathbf{F}^e(\tau)$ and the stress $\mathbf{T}^*(\tau)$:

$$\mathbf{F}^e(\tau) = \mathbf{F}(\tau) \mathbf{F}^p(\tau)^{-1}$$

$$\mathbf{T}^*(\tau) = \mathcal{C}[\mathbf{E}^e(\tau)].$$

Step 9. Update the variables $\{\mathbf{T}(\tau), s^i(\tau)\}$:

$$\mathbf{T}(\tau) = \mathbf{F}^e(\tau) \{ [\det \mathbf{F}^e(\tau)]^{-1} \mathbf{T}^*(\tau) \} \mathbf{F}^{e\text{T}}(\tau)$$

$$s^i(\tau) = s^i(t) + \sum_{j \in \mathcal{A}} h^{ij} \Delta\gamma^j, \quad i = 1, \dots, N,$$

Step 10. Update the accumulated shears due to twinning and the twin functions:

$$\Gamma^i(\tau) = \Gamma^i(t) + \Delta\gamma^i,$$

$$f^i(\tau) = \Gamma^i(\tau) / \gamma_0,$$

where the index i ranges over all the active twin systems.

Step 11. Rotate the lattice if a sufficiently large fraction of the grain has twinned. Let

$f(\tau) = \max \{f^i(\tau)\}$ denote the maximum value of the twin fraction, and let $\xi \in [0.2, 1]$ denote a random number. If $f(\tau) > \xi$, then set $\mathbf{Q}(\tau) = \mathbf{Q}(t)(\mathbf{R}^{tw}(t))^T$.

Step 12. Calculate the “texture” $(\mathbf{m}_t^i, \mathbf{n}_t^i)$:

$$\begin{aligned} \mathbf{m}_t^i &= \mathbf{F}^e(\tau)\mathbf{m}_0^i(\tau), \\ \mathbf{n}_t^i &= \mathbf{F}^{e-T}(\tau)\mathbf{n}_0^i(\tau). \end{aligned}$$

The single-crystal constitutive equations and the time-integration procedures described in this section have been implemented in the finite-element program ABAQUS/Explicit (1995) by writing a “user material” subroutine.

APPENDIX B

To find the active systems and the corresponding shear increments we need to solve the linear problem

$$Ax = b, \tag{30}$$

subject to constraints

$$x_i \geq 0. \tag{31}$$

We may solve this problem using a minimization scheme as follows. First, we construct a convex scalar function as a sum of discrepancy and penalty functions. The discrepancy function is defined as

$$U = (Ax - b)^T(Ax - b), \tag{32}$$

minimizing of which gives a solution of the linear system in the sense of least squares. To take into account the constraints (31), we must add to the function U a penalty function which helps in the satisfaction of the constraints. The form of penalty functions depends on the iterative minimization procedure. We choose the conjugate gradient method. This method converges to the minimum of the quadratic function in a finite number of steps. The main idea of the method is to choose a secant search direction in the subspace orthogonal to all the previous search directions. Two variants of this approach are the Fletcher–Powell (1963), and the Fletcher–Reeves (1964) algorithms. One of the simplest and effective classes of penalty functions is the “cut-type”:

$$F(x) = \begin{cases} 0 & \text{if condition is satisfied,} \\ g(x) & \text{otherwise,} \end{cases}$$

where $g(x)$ is a positive function increasing with x moving away from the domain where the condition is satisfied. We choose our penalty functions corresponding to the constraint (31) in the following form:

$$\Psi_i^2 = [\min(x_i, 0)]^2.$$

Together, the discrepancy and the penalty function may be written as

$$\tilde{U} = U + C\Sigma\Psi_i^2, \tag{33}$$

where C is a scalar weighting coefficient. Provided that the system, eqn (30), is not singular, the minimum of this function gives us the least square solution of the system, eqn (30), subject to the constraints (31). If A is singular, the paraboloid degenerates to a plane, and the system has an infinite number of solutions. Guided by the SVD method outlined in Appendix A,

we add another penalty term which guarantees a minimum length solution. With this, the minimization function becomes

$$U^* = U + C\Sigma\Psi_i^2 + W\Sigma(x_i)^2, \quad (34)$$

with gradient

$$G = 2A^T(Ax - b) + 2C\Psi + 2Wx. \quad (35)$$

Here W is another scalar weight coefficient. Since the last term should play a role only at the end of the solution process, and since it does not affect the solution if the matrix A is not singular, the weight W should be small in contrast to the weight C . The weight coefficients C and W , and the desired minimum value of the gradient $\|G\|$ are used to control the solution process.

The solutions obtained by either the minimization method outlined above, or the method based on the SVD decomposition of A , are identical. The advantage of the method outlined in this Appendix is that it avoids the iterative and repeated solution of the system $Ax = b$, using the SVD method to ensure that the constraints $x_i \geq 0$ are satisfied.